

The Cluster Mass Function from Early SDSS Data: Cosmological Implications

Neta A. Bahcall¹, Feng Dong¹, Paul Bode¹, Rita Kim², James Annis³, Timothy A. McKay⁴, Sarah Hansen⁴, Chris Miller⁶, Josh Schroeder¹, James Gunn¹, Jeremiah P. Ostriker¹, Marc Postman⁵, Robert C. Nichol⁶, Tomotsugu Goto⁶, Jon Brinkmann⁷, Gillian R. Knapp¹, Don O. Lamb⁸, Donald P. Schneider⁹, Michael S. Vogeley¹⁰, Donald G. York⁸

ABSTRACT

The mass function of clusters of galaxies is determined from 400 deg² of early commissioning imaging data of the Sloan Digital Sky Survey; ~ 300 clusters in the redshift range $z = 0.1 - 0.2$ are used. Clusters are selected using two independent selection methods: a Matched Filter and a red-sequence color magnitude technique. The two methods yield consistent results. The cluster mass function is compared with large-scale cosmological simulations. We find a best-fit cluster normalization relation of $\sigma_8 \Omega_m^{0.6} = 0.33 \pm 0.03$ (for $0.1 \lesssim \Omega_m \lesssim 0.4$), or equivalently $\sigma_8 = (\frac{0.16}{\Omega_m})^{0.6}$. The amplitude of this relation is significantly lower than the previous canonical value, implying that either Ω_m is lower than previously expected ($\Omega_m = 0.16$ if $\sigma_8 = 1$) or σ_8 is lower than expected ($\sigma_8 = 0.7$ if $\Omega_m = 0.3$)

¹Princeton University Observatory, Princeton, NJ 08544

²Department of Physics and Astronomy, The Johns Hopkins University, Baltimore, MD 21218

³Fermi National Accelerator Laboratory, P.O. Box 500, Batavia, IL 60510

⁴University of Michigan, Department of Physics, 500 East University, Ann Arbor, MI 48109

⁵Space Telescope Science Institute, Baltimore, MD 21218

⁶Department of Physics, Carnegie Mellon University, 5000 Forbes Avenue, Pittsburgh, PA 15213-3890

⁷Apache Point Observatory, 2001 Apache Point Road, P.O. Box 59, Sunspot, NM 88349-0059

⁸The University of Chicago, Department of Astronomy and Astrophysics, 5460 S. Ellis Ave., Chicago, IL 60637

⁹Department of Astronomy and Astrophysics, The Pennsylvania State University, University Park, PA 16802

¹⁰Department of Physics, Drexel University, Philadelphia, PA 19104

as suggested by recent results. The shape of the cluster mass function partially breaks this classic degeneracy; we find best-fit parameters of $\Omega_m = 0.19 \pm_{0.07}^{0.08}$ and $\sigma_8 = 0.9 \pm_{0.2}^{0.3}$. High values of Ω_m ($\gtrsim 0.4$) and low σ_8 ($\lesssim 0.6$) are excluded at $\gtrsim 2\sigma$.

Subject headings: cosmology:observations–cosmology:theory–cosmological parameters–dark matter–galaxies:clusters:general– large-scale structure of universe

1. Introduction

The abundance of clusters of galaxies as a function of mass places one of the strongest constraints on the amplitude of mass fluctuations on $8 h^{-1}$ Mpc scale, σ_8 , and on the mass density parameter, Ω_m . The present-day cluster mass function was the first observation to suggest that the standard $\Omega_m = 1$ Cold Dark Matter (CDM) model has to be highly biased, with $\sigma_8 \sim 0.5$ (i.e., a bias of ~ 2 , since the galaxy fluctuations amplitude is $\sigma_{8gal} \sim 1$), in order to match the observed cluster abundance. The cluster mass function also showed that low-density CDM models fit the cluster data well with little or no bias (i.e., $\sigma_8 \sim 1$) (Bahcall & Cen 1992; White, Efstathiou, & Frenk 1993). The mass function constraint, frequently called “cluster normalization” because of its powerful constraint on the linear mass power spectrum amplitude σ_8 , has provided the well known relation $\sigma_8 \Omega_m^{0.5} = 0.5 \pm 0.05$; this result was obtained from observations of both the cluster mass function (Bahcall & Cen 1992, 1993) and from the cluster temperature function (Edge et al. 1990; Henry & Arnaud 1991; White, Efstathiou, & Frenk 1993; Kitayama & Suto 1996; Eke, Cole, & Frenk 1996; Viana & Liddle 1996; Eke et al. 1998; Pen 1998; Markevitch 1998; Henry 2000). This relation implies that $\Omega_m \sim 0.3$ if $\sigma_8 \sim 0.9 - 1$; this latter value of σ_8 is suggested from other observations including cluster abundance evolution (Bahcall & Fan 1998; Donahue & Voit 2000, and references therein), the flattening of the mass-to-light ratio on large scales (Bahcall, Lubin, & Dorman 1995; Bahcall et al. 2000), and the SDSS and 2dF large scale structure observations (Szalay et al. 2002; Verde et al. 2002). Similar σ_8 - Ω_m normalization relations have been recently obtained from weak lensing observations on large scales (Van Waerbeke et al. 2001, 2002; Hoekstra et al. 2002; Bacon et al. 2002; Refregier et al. 2002, and references therein).

More recently, using new X-ray cluster samples and different virial mass versus temperature relations (which are critical for a precise determination of the cosmological constraints), cluster normalizations that are either considerably lower (by $\sim 2\sigma$; $\sigma_8 \Omega_m^{0.5} \simeq 0.4 \pm 10\%$) or higher ($\simeq 0.6 \pm 10\%$) than the above value have been reported (Borgani et al. 2001; Ikebe et al. 2002; Seljak 2002; Reiprich & Bohringer 2002; Viana, Nichol, & Liddle 2002; Pierpaoli et al. 2001; here we converted all the relations to the same power-law slope of 0.5

for easier comparison). An accurate determination of this parameter is important for two reasons. First, the normalization σ_8^2 enters exponentially in the evolution of structure in the universe; a 20% change in σ_8 has a significant (exponential) effect on the evolution of structure with time and, of course, on the amount of bias in the universe (i.e., how mass traces light). Second, if we know σ_8 or Ω_m from other observations, the above relation can be used to determine the second parameter. For example, if $\sigma_8 \sim 1$, as suggested by some observations, then the implied value of Ω_m differs by nearly a factor of two depending on whether the cluster normalization relation is $\sigma_8 \Omega_m^{0.5} = 0.6 \pm 10\%$ or $0.4 \pm 10\%$; these values imply $\Omega_m = 0.36 \pm 20\%$ or $0.16 \pm 20\%$, respectively.

Most of the previous analyses, which use the cluster temperature function, employ a smaller number of clusters, and assume a relation between virial cluster mass and temperature, which sensitively affects the results. The cosmological interpretations are generally based on comparisons with theoretical approximations such as the Press-Schechter formalism.

In this paper we use the early commissioning data from the Sloan Digital Sky Survey (SDSS: York et al. 2000; Stoughton, et al. 2002) to determine a preliminary mass function of nearby clusters of galaxies and derive its cosmological constraints. The data cover about 400 deg² with ~ 300 clusters at $z = 0.1 - 0.2$ from each of two independent samples (~ 600 clusters in total) — considerably larger than previous samples. The analysis does not use cluster virial masses, nor the virial mass temperature relation, which are more difficult to determine observationally. Rather, we use cluster masses observed within a fixed radius, as calibrated from the observed cluster luminosities and tested against cluster velocity dispersion. We use two independently selected cluster samples, identified by different algorithms — the Matched Filter method and the color-magnitude maxBCG method; we find consistent results for the two samples. We compare the results directly with large scale (Gpc³) cosmological simulations as well as with the Press-Schechter formalism to determine the cosmological constraints.

Finally, we note that the current results are based on a very small fraction (4%) of the ultimate SDSS 10⁴ deg² survey, which will yield thousands of clusters, many with velocity dispersions and weak gravitational lensing masses. The present mass function is therefore preliminary, intended to show the feasibility of using clusters from SDSS by utilizing the early commissioning data; larger and more accurate data will become available from SDSS in the near future.

2. Cluster Selection from SDSS Commissioning Data

The SDSS (York et al. 2000) is a 5-band CCD imaging survey that will cover, when complete, 10^4 deg² of the high latitude North Galactic Cap, and a smaller deeper region in the South, followed by an extensive multi-fiber spectroscopic survey. The imaging survey is carried out in drift-scan mode in five SDSS filters, u, g, r, i, z, to a limiting point source magnitude of $r < 23$ (Fukugita et al. 1996; Gunn et al. 1998; Lupton, et al. 2001; Hogg et al. 2001; Smith et al. 2002; Pier et al. 2002). The spectroscopic survey will target nearly one million galaxies to approximately $r < 17.7$, with a median redshift of $z \sim 0.1$ (Strauss, et al. 2002), and a smaller deeper sample of $\sim 10^5$ Luminous Red Galaxies to $r \sim 19$ and $z \sim 0.5$ (Eisenstein, et al. 2001).

In this paper we use 379 deg² of the early commissioning data of SDSS imaging, covering the area $\alpha(2000) = 355.0^\circ$ to 56.0° , $\delta(2000) = -1.25^\circ$ to 1.25° ; and $\alpha(2000) = 145.3^\circ$ to 236.0° , $\delta(2000) = -1.25^\circ$ to 1.25° (runs 94/125 and 752/756; Stoughton, et al. 2002). Clusters of galaxies were selected from these imaging data using, among others, a Matched-Filter method (Kim et al. 2002a,b) and an independent color-magnitude maximum-likelihood Brightest Cluster Galaxy method (maxBCG; Annis et al. 2002). These methods are briefly described below. A detailed comparison between these independent cluster selection methods and their properties is given in Bahcall et al. (2002). Here we use clusters selected from these techniques to determine a preliminary mass function of nearby clusters of galaxies.

The Matched Filter method HMF (Hybrid Matched Filter; Kim et al. 2002a) is a hybrid of the Matched Filter (Postman et al. 1996) and the Adaptive Matched Filter techniques (Kepner et al. 1999). This method identifies clusters in imaging data by finding peaks in a cluster likelihood map generated by convolving the galaxy survey with a filter based on a model of the cluster and field galaxy distribution. The cluster filter is composed of a projected density profile model for the galaxy distribution (Plummer law profile), and a luminosity function filter (Schechter function), using the typical parameters observed for galaxy clusters (within a radius of $1 h^{-1}$ Mpc). The HMF method identifies the highest likelihood clusters in the imaging data and determines their best-fit estimated redshift (z_{est}) and richness (Λ); the best-fit richness is proportional to the total cluster maximum likelihood luminosity within a radius of $1 h^{-1}$ Mpc. A relatively high threshold has been applied to the HMF cluster selection ($\sigma > 5.2$, Kim et al. 2002a); therefore, the selected clusters have typical richness of $\Lambda > 20-30$ (i.e., $L_{cl}(< 1 h^{-1} \text{ Mpc}) > 20 L^* \sim 2 \times 10^{11} h^{-2} L_\odot$). This threshold corresponds to clusters poorer than Abell richness class 0. (For more details see Kim et al. 2002a).

The maxBCG method (Annis et al. 2002) is based on the fact that the brightest cluster galaxy (BCG) generally lies in a narrowly defined space in luminosity and color (see, e.g,

Hoessel & Schneider 1985; Gladders & Yee 2000). For each SDSS galaxy, a BCG likelihood is calculated as a function of redshift based on the galaxy color ($g-r$ and $r-i$) and magnitude. The cluster likelihood is then weighted by the number of nearby red galaxies (located within $1 h^{-1}$ Mpc projected separation) that are within the color-magnitude region expected for the relevant cluster E/S0 galaxy ridgeline. This combined likelihood is used for cluster identification. The likelihood is calculated as a function of redshift from $z = 0$ to 0.5 , at 0.01 intervals. The best estimated redshift is that which maximizes the cluster likelihood. Since elliptical galaxies possess very regular colors, they provide excellent photometric redshift estimates for their parent clusters. The richness estimator, N_{gal} , is defined as the number of red E/S0 ridgeline member galaxies that are brighter than $M_i = -20.25$ (i.e., 1 mag fainter than L^* ; $h = 1$), and are located within a $1 h^{-1}$ Mpc radius of the BCG. (For more details see Annis et al. 2002).

The HMF cluster catalog contains clusters with richness $\Lambda > 20$ and redshift $z_{est} < 0.5$ (Kim et al. 2002a,b). The selection function for this sample has been determined using simulated clusters (see above references). The HMF redshift uncertainty is determined to be $\sigma_z = 0.03$ (by comparison with measured redshifts, Bahcall et al. 2002); the redshift uncertainty of the maxBCG clusters is $\sigma_z = 0.02$.

In this paper we determine the abundance of HMF clusters as a function of richness for nearby clusters ($z = 0.1 - 0.2$) and use the observed richness - mass relation to determine a preliminary mass function for the HMF clusters. A similar analysis is carried out for the independently selected maxBCG clusters and the results compared. Each of the independent samples contains ~ 300 clusters within the redshift ($z = 0.1 - 0.2$) and richness ($\Lambda \geq 30$ and $N_{gal} \geq 10$) limits used in this analysis.

3. The Cluster Mass Function

3.1. HMF Cluster Mass Function

We determine the mass function of nearby clusters of galaxies using HMF clusters with richness $\Lambda \geq 30$ and redshift $z = 0.1 - 0.2$. (At $z < 0.1$, the number of clusters is small and their selection less effective; we thus restrict our analysis to the above range.) To minimize false-positive detections we use the VC1 sample (Visually Confirmed sample, Kim et al. 2002a,b) which contains $> 80\%$ of all $\Lambda \geq 30$ HMF clusters, increasing to $> 90\%$ for $\Lambda \geq 50$ clusters. The total number of VC1 clusters observed within this redshift and richness range is 294 (uncorrected for selection function). Each cluster is corrected by the appropriate selection function for the given cluster richness and redshift as determined from cluster simulations

(Kim et al. 2002a). The cluster abundance as a function of richness, from $\Lambda \geq 30$ to $\Lambda \geq 70$, is obtained by dividing the above volume-limited corrected cluster count by the relevant volume ($z = 0.1 - 0.2$). A flat $\Omega_m = 0.3$ cosmology is assumed for the volume calculation, and a Hubble constant of $H_0 = 100 h \text{ km/s/Mpc}$ is used. (When fitting to different cosmologies in Section 4, the proper self-consistent cosmological volume is used for each Ω_m value.)

Two corrections are applied to the cumulative cluster richness function. First, we correct the abundance of clusters above a given richness, $n (\geq \Lambda)$, for the effect of redshift uncertainty in the HMF clusters, $\sigma_z = 0.03$ (see Section 2). The correction factor is determined using Monte Carlo simulations of realistic cluster distribution with redshift and richness, which is convolved with the observed Gaussian scatter in redshift, $\sigma_z = 0.03$. We find that the redshift uncertainty has a small effect, causing about 10% more clusters to be scattered into the $z = 0.1 - 0.2$ volume than are scattered out. We correct the cluster abundances downward by this small correction. Second, we correct the derived cluster abundance for the effect of uncertainty in the HMF richness, estimated to be 20% based on cluster simulations. We use Monte Carlo simulations with a realistic richness function, convolve it with the known observational selection function to produce the observed number of clusters as a function of true richness and then scatter the richness with the observed uncertainty to yield the observed richness function. Comparing the observed and true richness functions in 10^3 simulations we determine the proper correction factors and their dispersion, which we apply to the data. We find that the observed abundances are larger than the true ones, as expected due to the excess scatter of the more numerous low richness clusters to higher richness; this effect is 10% at $\Lambda \sim 30 - 40$, increasing to 35% - 55% at $\Lambda \sim 60 - 70$. We correct the cluster abundances for this effect, and use the observed variance in the final error analysis discussed below.

The uncertainties in the observed cluster abundance include the statistical uncertainties ($N^{\frac{1}{2}}$), the uncertainties in the selection function ($\pm 15\%$) and in the false-positive correction ($\pm 15\%$), and the uncertainties derived from the Monte Carlo simulations for each of the two corrections above (the redshift correction factor has an uncertainty of 4% to 42% for the range $\Lambda \geq 30$ to $\Lambda \geq 70$, and the richness correction factor has an uncertainty of 3% to 23% for the same range).

To determine a cluster mass function from the above cluster richness function we need to convert the cluster richness thresholds to a mean cluster mass. Throughout this paper we use cluster mass within a given fixed radius (not virial mass); this mass is more accurately obtained from observations since the virial radius is not precisely known. We convert richness to mass in two independent ways, both from observations. First, we use the mean cluster luminosity measured in the SDSS data for all clusters stacked as a function of their richness. The cluster luminosity is observed within a radius of $0.6 h^{-1} \text{ Mpc}$, in the r-band, for galaxies

brighter than $M_r = -19.8$ (K-corrected for each galaxy type following Fukugita et al. 1996), and corrected for a similarly determined local background in five separate locations (which allows us to account for the variance in the background correction; Hansen et al. 2002; Bahcall et al. 2002). We use the mean observed cluster luminosity $L_{0.6}$ for clusters with richness threshold of $\Lambda=30, 40, 45, 50, 60$ and 70 . The observed mean luminosity $L_{0.6}$ of the stacked clusters is presented as a function of richness in Figure 1. We note that any biases or uncertainties in the richness parameter (e.g., Kim et al. 2002a) are calibrated out in this procedure since the actual mean cluster luminosities are directly measured by this method. The richness parameter serves only as a tracer; a richness bias will properly calibrate itself by the measured mean luminosity (as is in fact seen by the non-linear relation between $L_{0.6}$ and Λ). The cluster luminosity is corrected to include the unobserved faint-end of the cluster luminosity function, that is, all galaxies fainter than $M_r = -19.8$. For the observed SDSS Schechter luminosity function parameters of the HMF clusters (within $0.6 h^{-1}$ Mpc), $\alpha = -1.08 \pm 0.01$ and $M_r^* = -21.1 \pm 0.02$ (Hansen et al. 2002; see also Goto et al. 2002; $h = 1$), we adopt a correction factor of 1.42 ± 0.08 for the added contribution of faint galaxies to the total HMF cluster luminosity. The cluster mean luminosity is then converted to cluster mass, $M(< 0.6 h^{-1}$ Mpc physical), using the mean observed cluster M/L_r ratio for each richness threshold (Bahcall & Comerford 2002). The observed best-fit M/L is used (based on the means of 20 clusters and 33 groups): $M/L_{v,tot}$ ($z=0$) = $142 \pm 32 + (23 \pm 5) T_{kev} h$ (Bahcall & Comerford 2002). The mild increase of M/L with temperature, T_{kev} (seen both in observations and in simulations, e.g., Bahcall et al. 2000), is accounted for at each richness threshold using the observed correlation between richness and velocity dispersion (see below) and the observed mean relation between velocity dispersion and temperature ($\sigma_v = 332 T_{kev}^{0.6} km s^{-1}$, Lubin & Bahcall 1993). This effect is small for the range of cluster temperatures studied here ($T \simeq 0.9$ to 4 keV). The mean observed $M/L_{v,tot}$ at $z=0$ is converted to M/L_r (where L_r is the relevant SDSS Petrosian r luminosity) using the conversions given by Fukugita et al. (1996), Bahcall & Comerford (2002), Strauss, et al. (2002). We use $L_r = 0.85 L_{r,tot}$ (Strauss, et al. 2002, for $\sim 60 - 70\%$ of cluster light contributed by early type galaxies), $M/L_{r,tot} = 0.94 M/L_{v,tot}$, and M/L_r ($z = 0.17$) = $0.943 M/L_r$ ($z = 0$) (Carlberg et al. 1997a; Bahcall & Comerford 2002). The above yields M/L_r values (at $z=0.17$) that range from 170 at $\Lambda \geq 30$ to 235 at $\Lambda \geq 70$. The mean mass of clusters (within $0.6 h^{-1}$ Mpc) is then determined for the relevant richness thresholds ($\Lambda \geq 30$ to $\Lambda \geq 70$).

The uncertainties in the mean mass estimates are derived from the combined uncertainties in the observed mean luminosity-richness relation, the uncertainty in the observed mean M/L ratio, and the smaller uncertainties in the corrections applied above. In order to determine the proper uncertainties in the luminosity-richness relation that are relevant for the mean cluster mass estimates, we generate 10^3 Monte Carlo simulations with a realistic

L- Λ relation and richness function. We introduce a Gaussian redshift scatter of $\sigma_z = 0.03$ as well as a $\sim 20\%$ to 30% uncertainty in individual cluster luminosities. We recover the mean "observed" L- Λ relation from the 10^3 simulations and the mean luminosities at the relevant cluster richness thresholds (for the observed redshift range). The recovered mean relation is consistent with the input L- Λ relation. The derived 1σ variance in the recovered L- Λ relation from the simulations ranges from 11% at $\Lambda=30$ to 25% at $\Lambda=70$. We use these uncertainties in estimating cluster mass uncertainties. The uncertainty in the mean observed M/L ratio, 15% for the relevant cluster richnesses, is combined with an additional 8% uncertainty in the conversion factors described above and a 6% uncertainty in the luminosity function faint end extrapolation (see above). The mass uncertainties thus range from 20% at $\Lambda\sim 30$ to 31% at $\Lambda\sim 70$. The cluster abundances have been corrected for this scatter using Monte Carlo simulations, as described above for the richness-function abundance correction.

For comparison with other commonly used cluster masses, as well as for direct comparison with available cosmological simulations, we also determine the mass function for cluster masses within two additional frequently used radii: the slightly smaller radius of $0.5 h^{-1}$ Mpc, using the observed mean luminosities $L_{0.5}$, and, for illustration purposes, also the larger comoving radius of $1.5 h^{-1}$ Mpc; the latter is obtained by extrapolating the $0.6 h^{-1}$ Mpc luminosity to $1.5 h^{-1}$ Mpc comoving radius ($= 1.28 h^{-1}$ Mpc at $z = 0.17$) using the typical observed luminosity profile in clusters ($\rho_L \sim R^{-2}$ for $R < R_{200}$ and $\sim R^{-2.4}$ for $R \gtrsim R_{200}$, where R_{200} is the radius within which the cluster overdensity is 200 times the critical density; Carlberg et al. 1997b; Fischer & Tyson 1997).

These two mass functions are compared in Figure 2 with the mass function obtained from large-scale cosmological simulation (Bode et al. 2001) of the concordance LCDM model (Bahcall et al. 1999): $\Omega_m = 0.3$, $\Lambda = 0.7$, $\sigma_8 = 0.9$ (i.e. $\sigma_8 \Omega_m^{0.5} = 0.49$), and $h = 0.67$. This simulation used a $1 h^{-1}$ Gpc box size and 1024^3 dark matter particles, with a particle mass of $2.3 \times 10^{10} h^{-1} M_\odot$, and softening length of $14 h^{-1}$ Kpc (Bode et al. 2001). Such a large box ensures a statistically valid sample of simulated clusters, and the high particle number ensures that the clusters are well resolved — for the smallest clusters considered here there are over 10^3 particles within $0.5 h^{-1}$ Mpc. The details of the simulation and the method of computing the mass function are described in Bode et al. (2001). The simulated mass function is presented as a function of $M(< 0.5 h^{-1}$ Mpc physical) and $M(< 1.5 h^{-1}$ Mpc comoving) at $z = 0.17$, for direct comparison with the observations. Figure 2 shows that the shape of the SDSS mass function agrees well with that expected from the cosmological simulations but the normalization is significantly lower than expected from the concordance model. The best-fit function, with a lower σ_8 - Ω_m amplitude, is also presented in Figure 2; it is discussed in Section 4.

The observed HMF cluster mass function for $M(<0.6 h^{-1} \text{ Mpc})$ is presented in Figure 3. As a further consistency test, we estimate mean cluster masses using an entirely independent method: the observed correlation between mean cluster richness and cluster velocity dispersion. We use cluster velocity dispersions of 19 clusters determined from the SDSS spectroscopic survey (for clusters with ~ 30 to 160 redshifts) as well as from several Abell clusters available in the literature (Mazure et al. 1996; Slingsend et al. 1998; Abell 168, 295, 957, 1238, 1367, 2644). Even though the number of clusters with measured velocity dispersion is not large and the scatter considerable, a clear correlation between median velocity dispersion and richness is observed, as expected; we find a best-fit relation $\sigma_v(\text{km s}^{-1}) \simeq 10.2 \Lambda$. We estimate mean cluster mass (within $0.6 h^{-1} \text{ Mpc}$) from this relation and use it to illustrate consistency with the mass function determined from the entirely independent cluster luminosity method discussed above. We use the observed relation between cluster mass and cluster velocity dispersion derived from observations of weak gravitational lensing of clusters: $M(< 0.6 h^{-1} \text{ Mpc}) = 0.0717 k_\delta \sigma_{100}^{1.67} 10^{14} h^{-1} M_\odot$ (where σ_{100} is in 100 km s^{-1} ; Hjorth et al. 1998; also Bahcall & Sette 2002). This relation is obtained from the observed relations $M/R = 0.88 k_\delta T(\text{keV})$ for $R < 1 h^{-1} \text{ Mpc}$, where k_δ is the small overdensity correction factor ($k_\delta = 0.76, 0.9, 1, 1.1, 1.15$, respectively, for cluster overdensity of $\delta = 100, 250, 500, 1000, 2500$; see references above and Evrard et al. 1996), and $\sigma_v(\text{km s}^{-1}) = 332 T_{kev}^{0.6}$ (Lubin & Bahcall 1993). The cluster mass function determined from this independent method, performed as a consistency check, is in full agreement with the mass function determined earlier using cluster luminosities; the results are compared in Figure 3. The velocity dispersion comparisons from the two methods — i.e., the velocities inferred from the cluster luminosity-mass method and the directly observed velocity dispersions are shown as a function of richness in Figure 4. The excellent agreement between these two independent methods supports the mass determination discussed above.

3.2. maxBCG Cluster Mass Function

For comparison, we also determine the cluster mass function from the independently selected maxBCG clusters. This method uses a completely independent selection criterion: the maxBCG selection technique assumes no cluster filters or profiles; rather, it selects clusters based on the red colors and magnitudes of the brightest cluster galaxies (Section 2). A comparison of the two mass functions can therefore provide further support for the above results.

We follow the same procedure for the maxBCG clusters as described above for the HMF clusters. We use the observed mean luminosity $L_{0.6}$ of all stacked maxBCG clusters

as a function of richness, N_{gal} (where N_{gal} is the maxBCG cluster richness, Section 2); the data are presented in Figure 1. We extrapolate the luminosity to the faint-end of the cluster luminosity function (within $0.6 h^{-1}$ Mpc; $\alpha = -1.05 \pm 0.01$, $M_r^* = -21.25 \pm 0.02$ for the maxBCG clusters for $h = 1$, Hansen et al. 2002; see also Goto et al. 2002), yielding a correction factor of 1.34 ± 0.06 , and convert the cluster luminosity to mean cluster mass using the mean observed M/L ratios. All maxBCG clusters (357 clusters) with richness $N_{gal} \geq 10$ (comparable in richness to HMF clusters with richness $\Lambda \gtrsim 30$; Bahcall et al. 2002) in the redshift range $z = 0.1 - 0.2$ are used. Corrections and uncertainties are calculated as described above (with $\sigma_z = 0.02$, $\Delta N_{gal} = 10\% - 15\%$). The selection function and the false-positive correction factor for the $N_{gal} \geq 10$ maxBCG clusters at $z = 0.1 - 0.2$ are estimated from simulations to be $\sim 0.9 - 1 \pm 15\%$ each. The fraction of HMF clusters that are found by the maxBCG method is 61% (for maxBCG matches with $N_{gal} \geq 6$ located within $1 h^{-1}$ Mpc projected separation). This is consistent with the maxBCG selection function ($\sim 85\%$ for $N_{gal} \geq 6$), the HMF false-positive detection rate ($\sim 20\%$, for $\Lambda \geq 30$), and the smaller correction due to redshift uncertainty (see Bahcall et al. 2002). The overlap rate decreases considerably if only $N_{gal} \geq 10$ maxBCG matches are considered for the HMF clusters (within $1 h^{-1}$ separation and ± 0.05 in redshift). This is as expected due to the large scatter of clusters across the richness threshold; Monte Carlo simulations indicate that a richness cut reduces the overlap by $\sim 55\% - 60\%$ (Bahcall et al. 2002).

There are 58 Abell clusters located within the current survey area; all 58 clusters are detected by the combined HMF and maxBCG clusters (maxBCG finds all 58 clusters; HMF finds 49 of the 58 clusters, consistent with the respective selection functions). A few of the clusters are detected below the thresholds used here (i.e., $\Lambda < 30$, $N_{gal} < 10$, $z < 0.1$, or $z > 0.2$). In addition, there are 5 X-ray clusters from the XBACs sample (Ebeling et al. 1996) located within the survey region. All 5 are detected by the HMF and maxBCG methods.

The maxBCG cluster mass function is presented in Figure 5; it is superposed, for comparison, on the HMF mass function from Figure 3. A good agreement between the two independent mass functions is observed. This agreement provides further support to the above estimate of the SDSS cluster mass function. In addition, we use the best-fit relation observed between mean cluster velocity dispersion and richness for maxBCG clusters (21 clusters with measured dispersions) as an additional test; the observed median relation, $\sigma_v(\text{km/s}) = 93 N_{gal}^{0.56}$ (Figure 4), is used to independently estimate cluster masses using $M(< 0.6 h^{-1} \text{ Mpc}) = 0.0717 k_\delta \sigma_{100}^{1.67} 10^{14} h^{-1} M_\odot$, as described above. The results of the two methods (Figure 5) are consistent with each other.

We can compare the observed cluster mass function with the recently observed cluster temperature function by Ikebe et al. (2002). For this purpose we use the observed relation

discussed above, $M (< 0.6 h^{-1} \text{ Mpc}) = 0.53 k_{\delta} T(\text{keV}) 10^{14} h^{-1} M_{\odot}$, to derive an approximate temperature function from the above mass function. We find a good agreement between the mass function (based on 300 clusters at $z = 0.1 - 0.2$) and the Ikebe et al. temperature function (based on 60 X-ray clusters, mostly at $z < 0.1$) (accounting for the slightly higher redshift of the SDSS sample, in accord with cosmological simulations; Bode et al. 2001). The SDSS mass function reaches to poorer clusters, of lower temperature ($T \sim 1 \text{ keV}$), as compared with the X-ray temperature function ($T > 2 \text{ keV}$); because of the small area covered, the current SDSS sample does not contain the most massive clusters— these highest mass clusters will become available as the sample size increases. The agreement between these independent determinations provides further support of the current cluster mass function results.

4. Cosmological Implications

The cluster mass function places one of the most powerful constraints on the cosmological parameters Ω_m and σ_8 ; it determines the important cluster normalization relation, i.e., the value of σ_8 as a function of Ω_m .

Early data of the cluster mass function (Bahcall & Cen 1992), and the cluster temperature function (Henry & Arnaud 1991; White, Efstathiou, & Frenk 1993; Eke, Cole, & Frenk 1996; Eke et al. 1998; Pen 1998), provided a cluster normalization relation of $\sigma_8 \Omega_m^{0.5} \simeq 0.5$ ($\pm \sim 10\%$; see above references for details). This powerful relation implies that for $\sigma_8 \sim 1$, $\Omega_m \sim 0.25$ (with slight differences depending on a flat versus open cosmology). For $\Omega_m = 1$, the required normalization of $\sigma_8 = 0.5$ implies a strong bias which is not supported by observations (Bahcall, Lubin, & Dorman 1995; Bahcall et al. 2000; Bahcall & Fan 1998; Feldman et al. 2001; Verde et al. 2002; Lahav et al. 2002).

More recently, using different X-ray cluster samples and different relations between virial mass and cluster temperature, a somewhat lower normalization value has been suggested (Borgani et al. 2001; Ikebe et al. 2002; Seljak 2002; Reiprich & Bohringer 2002; Viana, Nichol, & Liddle 2002), although higher values have also been reported (Pierpaoli et al. 2001). In this section we compare the preliminary mass function of SDSS clusters with analytic predictions to determine the best-fit cosmological parameters.

The mass function for a given cosmology can be predicted using the analytic formalism of Press & Schechter (1974), as in for example Eke, Cole, & Frenk (1996); Kitayama & Suto (1996); Viana & Liddle (1996); Henry (2000); and Reiprich & Bohringer (2002). While fairly successful in matching the results of N-body simulations, the standard P-S formalism

tends to predict too many low mass clusters and too few higher mass clusters. An improved fitting formula which better reproduces the results of N-body simulations is given by Jenkins et al. (2001); we will use this in preference to the standard P-S formula.

For a given set of cosmological parameters, we begin by calculating the linear matter power spectrum using the publicly available CMBFAST code (Seljak & Zaldarriaga 1996). Knowing the power spectrum, we calculate the variance of the linear density field and thus find the mass function with equation B3 of Jenkins et al. (2001). As Hu & Kravtsov (2002) show, this formula is appropriate for a definition of cluster mass within a sphere enclosing a mean overdensity which is a fixed multiple of the mean density. Because the HMF and maxBCG masses are instead derived within a fixed radius (independent of density or mass), we adjust the analytic masses using the mass distribution corresponding to the NFW density profile (Navarro, Frenk, & White 1997), which provides an accurate representation of N-body results. To do this we follow the method presented in the Appendix of Hu & Kravtsov (2002).

The resulting analytic prediction, using cluster mass within two different radii of $0.5 h^{-1}$ Mpc (physical) and $1.5 h^{-1}$ Mpc (comoving), is shown for the concordance model in Figure 2 as a dotted line. This analytic function is in excellent agreement with the direct N-body simulation (dashed line) over the relevant range of masses (though at higher or lower masses the agreement may not be so close).

To determine the best-fit mass function and the implied values of Ω_m and σ_8 , we compare the differential binned mass function to the above theoretical prediction using a standard χ^2 procedure. The last data point in each sample is not included in the best χ^2 fit determinations since this point contains only a few clusters (~ 7) with considerably less well determined mass. Only spatially flat models are considered. The Hubble constant is kept fixed at $H_0 = 72 \text{ km s}^{-1} \text{ Mpc}^{-1}$ (Freedman et al. 2001), with a baryon density of $\Omega_b h^2 = 0.02$ (Burles, Nollett, & Turner 2001), and CMB temperature $T_{CMB} = 2.726$ (Mather et al. 1994). We assume a primordial power spectral index $n = 1$.

The results, presented in Figures 2, 3 and 5, show a good agreement between the shape of the observed and theoretical LCDM mass function, but the observed function has a significantly lower normalization than the canonical value of $\sigma_8 \Omega_m^{0.5} = 0.5$ (the latter indicated by the dashed and dotted curves in Figure 1, representing the concordance LCDM model with $\Omega_m = 0.3$ and $\sigma_8 = 0.9$). Model simulations with a somewhat lower value of $\sigma_8 \Omega_m^{0.5} \simeq 0.45$ (for a flat Quintessence model and Open CDM, see Bode et al. 2001; not shown here to avoid crowding) also exhibit higher normalization than observed.

The best-fit mass function is presented in Figures 2 and 3 for the HMF clusters, and in Figure 5 for both the maxBCG and HMF clusters; the two independent best fit functions yield

similar results (Figure 5). The cosmological constraints derived from the χ^2 minimization are summarized in Figure 6, showing the allowed parameter range of Ω_m - σ_8 for both the HMF and the maxBCG samples. The best-fit parameters are $\Omega_m = 0.175 \pm_{0.07}^{0.08}$, $\sigma_8 = 0.92 \pm_{0.20}^{0.25}$ ($1\text{-}\sigma$) for the HMF clusters, and $\Omega_m = 0.195 \pm_{0.07}^{0.09}$, $\sigma_8 = 0.9 \pm_{0.2}^{0.3}$ for the maxBCG clusters (Figures 2, 3 and 5). The best-fit contours in Figure 6 show that high values of $\Omega_m (> 0.4)$ and low values of $\sigma_8 (< 0.6)$ are ruled out by the data at $\gtrsim 2\text{-}\sigma$; these yield mass functions that are too steep compared to the data. On the other hand, low values of Ω_m (down to ~ 0.1) and high values of σ_8 (up to ~ 1.2) are supported by the data. These results are obtained using the $M(< 0.6 h^{-1} \text{ Mpc})$ mass functions; similar results are obtained with $M(< 1.5 h^{-1} \text{ Mpc comoving})$.

The mean best-fit parameters of the observed mass function (with $1\text{-}\sigma$) are:

$$\Omega_m = 0.19 \pm_{0.07}^{0.08} \tag{1}$$

$$\sigma_8 = 0.9 \pm_{0.2}^{0.3} \tag{2}$$

The best-fit normalization relation (Figure 6) is:

$$\sigma_8 \Omega_m^{0.6} = 0.33 \pm 0.03 \quad (0.1 \lesssim \Omega_m \lesssim 0.4) \tag{3}$$

or, equivalently,

$$\sigma_8 = \left(\frac{0.16}{\Omega_m}\right)^{0.6} \pm 10\% \quad . \tag{4}$$

For comparison with previous results, this relation (3) is 20% lower than the standard normalization value of $\sigma_8 \Omega_m^{0.5} = 0.5$ (or similarly, $\sigma_8 \Omega_m^{0.6} \simeq 0.44$). As discussed earlier, this conclusion has a non-negligible implication for σ_8 and Ω_m as seen in equations (1) and (2) for the best-fit parameters (and discussed below).

The results are consistent with the recent temperature function results of Ikebe et al. (2002) and Seljak (2002). The higher amplitude obtained by some of the earlier work is most likely due to a combination of factors including use of the uncertain and sensitive theoretical (rather than observational) mass-temperature relation (when applied to X-ray clusters), smaller sample size, and overestimated cluster abundance (in some optical samples). Recent weak lensing observations on large scales yield results that range from $\sigma_8 \Omega_m^{0.5} \sim 0.4$ to 0.6 (or $\sigma_8 \Omega_m^{0.6} \sim 0.34$ to 0.52 when converted to a power law slope of 0.6, at $\Omega_m \sim 0.25$, for easier comparison; see references in Section 1); the low end of this range is consistent with the current results, but the high normalization values reported are inconsistent at the $2\text{-}\sigma$ level. A complementary analysis of the maxBCG cluster halo occupation function (Annis et al., in preparation) yields consistent results with those obtained above.

Our best-fit $\sigma_8\text{-}\Omega_m$ constraints are compared with previous results in Figure 7. This comparison illustrates the agreement of recent temperature function results with the current constraints, and shows the wide range among the earlier, higher $\sigma_8(\Omega_m)$ normalization results. The weak lensing analyses yield constraints that lie mostly at the higher $\sigma_8(\Omega_m)$ range; the lensing results of Hoekstra et al. (2002) are consistent with our current constraints.

This new cluster normalization has important implications for Ω_m . It is frequently assumed that Ω_m is 0.3, and the above relation is used to determine σ_8 (thus typically referred to as "low normalization", implying a lower than expected σ_8 value for $\Omega_m = 0.3$). However, the value of Ω_m is not accurately known, and could be as low as ~ 0.15 (see, e.g., Bahcall et al. 2000). At the same time, there are several measurements that suggest that $\sigma_8 \simeq 0.9 - 1$. This "high" normalization is obtained from the very mild evolution observed in the cluster abundance to $z \sim 1$ (Bahcall & Fan 1998; Donahue & Voit 2000); the flattening of the M/L function on large scales (Bahcall, Lubin, & Dorman 1995; Bahcall et al. 2000); SDSS observations of the galaxy power spectrum on large scales (Szalay et al. 2002); and the observation of no-bias in the galaxy distribution in the 2dF and infrared surveys (Verde et al. 2002; Feldman et al. 2001; but see, however, Lahav et al. 2002). This observationally suggested normalization of $\sigma_8 \simeq 0.9 - 1$ is fully consistent with our best-fit value for the SDSS cluster mass function (equations 1 and 2); it implies a low mass density of $\Omega_m \simeq 0.19$. This is also consistent with the low Ω_m value indicated by the M/L function on large scales.

5. Conclusions

We determine the mass function of nearby clusters of galaxies using ~ 300 clusters at $z = 0.1 - 0.2$ selected from $\sim 400 \text{ deg}^2$ of early SDSS commissioning data. Two independent cluster samples are used based on the Matched Filter and the color-magnitude maxBCG methods. The two samples yield consistent results. The analysis uses cluster masses within a fixed radius. The mass function is compared directly with large, Gpc^3 cosmological simulations. We find a best-fit cluster normalization relation of $\sigma_8\Omega_m^{0.6} = 0.33 \pm 0.03$, or equivalently $\sigma_8 = (\frac{0.16}{\Omega_m})^{0.6} \pm 10\%$. This result is significantly lower than the previous canonical value of $\sigma_8\Omega_m^{0.5} = 0.5 \pm 0.05$. The shape of the cluster mass function partially breaks this degeneracy; we find best-fit parameters of $\Omega_m = 0.19 \pm_{0.07}^{0.08}$ and $\sigma_8 = 0.9 \pm_{0.2}^{0.3}$. These values are consistent with the independent observationally suggested normalization of $\sigma_8 \simeq 0.9 - 1$ observed from cluster abundance evolution (Bahcall & Fan 1998; Donahue & Voit 2000), the flattening of the M/L function on large scales (Bahcall et al. 2000), and SDSS, 2dF, and infrared large-scale structure observations (Szalay et al. 2002; Verde et al. 2002; Feldman et al. 2001).

These preliminary results from early commissioning data of 4% of the ultimate SDSS survey will be greatly improved as additional SDSS data become available for thousands of clusters, many with measured velocity dispersions and weak lensing masses. Improvements in the sample size and accuracy, and in the relevant scaling relations are needed in order to achieve greater precision in the determination of the mass function and its cosmological implications.

The Sloan Digital Sky Survey is a joint project of The University of Chicago, Fermilab, the Institute for Advanced Study, the Japan Participation Group, The Johns Hopkins University, Los Alamos National Laboratory, the Max-Planck-Institute for Astronomy (MPIA), the Max-Planck-Institute for Astrophysics (MPA), New Mexico State University, Princeton University, the United States Naval Observatory, and the University of Washington. Apache Point Observatory, site of the SDSS telescopes, is operated by the Astrophysical Research Consortium (ARC). Funding for the project has been provided by the Alfred P. Sloan Foundation, the SDSS member institutions, the National Aeronautics and Space Administration, the National Science Foundation, the Department of Energy, the Japanese Monbukagakusho, and the Max Planck Society. The SDSS Web site is <http://www.sdss.org>.

REFERENCES

- Annis, J., et al. 2002 (maxBCG Cluster Catalog), in preparation
- Bacon, D., Massey, R. J., Refregier, A. R., & Ellis, R. S. 2002, MNRAS, submitted (astro-ph/0203134)
- Bahcall, N. A. & Cen, R. 1992, ApJ, 398, L81
- Bahcall, N. A. & Cen, R. 1993, ApJ, 407, L49
- Bahcall, N. A., Lubin, L. M., & Dorman, V. 1995, ApJ, 447, L81
- Bahcall, N. A. & Fan, X. 1998, ApJ, 504, 1
- Bahcall, N. A., Ostriker, J. P., Perlmutter, S., & Steinhardt, P. 1999, Science, 284, 1481
- Bahcall, N. A., Cen, R., Davé, R., Ostriker, J. P., & Yu, Q. 2000, ApJ, 541, 1
- Bahcall, N. A. et al. 2002, to be submitted
- Bahcall, N. A. & Comerford, J. 2002, ApJ, 565, 5
- Bahcall, N. A. & Sette, A. 2002, PU Junior project (in preparation for publication)

- Blanton, M. et al., & SDSS collaboration 2001, *AJ*, 121, 2358
- Bode, P., Bahcall, N. A., Ford, E. B., Ostriker, J. P., 2001, *ApJ*, 551, 15
- Borgani, S., et al. 2001, *ApJ*, 561, 13
- Burles, S., Nollett, K. M., & Turner, M. S. 2001, *ApJ*, 552, L1
- Carlberg, R. G., Yee, H. K. C., & Ellingson, E. 1997a, *ApJ*, 478, 462
- Carlberg, R. G. et al. 1997b, *ApJ*, 479, L19
- Donahue, M. & Voit, G. M. 1999, *ApJ*, 523, L137
- Ebeling, H., Voges, W., Bohringer, H., Edge, A. C., Huchra, J. P., & Briel, U. G. 1996, *MNRAS*, 281, 799E
- Edge, A. C., Stewart, G. C., Fabian, A. C., & Arnaud, K. A. 1990, *MNRAS*, 245, 559
- Eisenstein, D., et al., & SDSS collaboration 2001, *AJ*, 122, 2267
- Eke, V. R., Cole, S., & Frenk C. S. 1996, *MNRAS*, 282, 263
- Eke, V. R., Cole, S., Frenk, C. S. & Patrick H. J. 1998 *MNRAS*, 298, 1145
- Eke, V. R., Navarro, J. F., & Steinmetz, M. 2001, *ApJ*, 554, 114
- Evrard, A. E., Metzler, C. A., Navarro, J. F. 1996, *ApJ*, 469, 494
- Feldman, H. A., Frieman, J. A., Fry, J. N., Scoccimarro, R., 2001, *Phys. Rev. Letters*, 86, 1434 (astro-ph/0010205)
- Fischer, P. & Tyson, J. A. 1997, *AJ*, 114, 14
- Freedman, W. L., Madore, B. F., Gibson, B. K., et al. 2001, *ApJ*, 553, 47
- Fukugita, M., Ichikawa, T., Gunn, J. E., Doi, M., Shimasaku, K., & Schneider, D. P. 1996, *AJ*, 111, 1748
- Gladders, M. D. & Yee, H. K. C. 2000, *AJ*, 120, 2148
- Goto, T., et al. 2002, *AJ*, to be submitted
- Gunn, J. E. et al. 1998, *AJ*, 116, 3040
- Hansen, S. et al. 2002, in preparation

- Henry, J. P. 2000, ApJ, 534, 565
- Henry, J. P., & Arnaud, K. A. 1991, ApJ, 372, 410
- Hjorth, J., Oukbir, J. & van Kampen, E. 1998, MNRAS, 298, 1
- Hoekstra, H. et al. 2002, ApJ, submitted (astro-ph/0202285)
- Hoessel, J. G., & Schneider, D. P. 1985, AJ, 90, 1648
- Hogg, D. W. et al. 2001, AJ, 122, 2129
- Hu, W., & Kravtsov, A.V. 2002, ApJ, submitted (astro-ph/0203169)
- Ikebe, Y., Reiprich, T. H., Böhinger, H., Tanaka, Y. & Kitayama, T. 2002, A&A, 383, 773
- Jenkins, A., Frenk, C. S., White, S. D. M., Colberg, J. M., Cole, S., Evrard, A. E. & Yoshida, N. 2001, MNRAS, 321, 372
- Kepner, J., Fan, X., Bahcall, N. A., Gunn, J., Lupton, R., & Xu, G. 1999, ApJ, 517, 78
- Kim, R., et al. 2002a, AJ, 123, 20
- Kim, R., et al. 2002b (HMF Cluster Catalog), in preparation
- Kitayama, T., & Suto, Y. 1996 ApJ, 469, 480
- Lahav, O. et al., & 2dFGRS team 2002, MNRAS, in press (astro-ph/0112162)
- Lubin, L. M., Bahcall, N. A., 1993, ApJ, 415, L17
- Lupton, R., et al. 2001, ASP Conference Series, Vol. 238
- Markevitch, M., 1998, ApJ 504, 27
- Mather, J. C., et al. 1994, ApJ, 420, 439
- Mazure, A., et al. 1996, A&A, 310, 31
- Nakamura, T. T., & Suto, Y. 1997, Prog. Theor. Phys., 97, 49
- Navarro, J. F., Frenk, C. S. & White, S. D. M. 1997, ApJ, 490, 493
- Oukbir, J., & Arnaud, M. 2001, MNRAS, 326, 453
- Pen U. 1998, ApJ, 498, 60

- Pier, J. R. et al. 2002, AJ, submitted
- Pierpaoli, E., Scott, D. & White, M. 2001 MNRAS 325, 77
- Postman, M., Lubin, L. M., Gunn, J. E., Oke, J. B., Hoessel, J. G., Schneider, D. P., & Christensen, J. A. 1996, AJ, 111, 615
- Press, W. H., & Schechter, P. 1974, ApJ, 187, 425
- Proty Wu, J.-H. 2001, MNRAS, 327, 629
- Refregier, A., Rhodes, J., & Groth, E., 2002, ApJL, submitted (astro-ph/0203131)
- Reiprich, T. H., & Bohringer, H. 2002, ApJ, 567, 716
- Seljak, U., & Zaldarriaga, M. 1996, ApJ, 469, 437
- Seljak, U., MNRAS, submitted (astro-ph/0111362)
- Slinglend, K., Batuski, D., Miller, C., Haase, S., Michaud, K., Hill, J. M., 1998, ApJS, 115, 1S
- Smith, J. A. et al. 2002, AJ, 123, 2121
- Stoughton, C., et al. 2002, AJ, 123, 485
- Strauss, M., et al. 2002, AJ, submitted
- Szalay, A. et al., & SDSS collaboration, 2002, ApJ, in press (astro-ph/0107419)
- Van Waerbeke, L. et al. 2001, A&A, 374, 757
- Van Waerbeke, L., Mellier, Y., Pello, R., Pen, U-L., McCracken, H. J., & Jain, B. 2002, A&A, submitted (astro-ph/0202503)
- Verde, L. et al., & 2dFGRS team 2002, MNRAS, submitted (astro-ph/0112161)
- Viana, P. P., & Liddle, A. R. 1996, MNRAS, 281, 323
- Viana, P. P., Nichol, R., & Liddle, A. R., 2002, ApJ submitted (astro-ph/0111394)
- White, S. D. M., Efstathiou, G., & Frenk, C. S. 1993, MNRAS, 262, 1023
- York, D. G. et al., & SDSS collaboration 2000, AJ, 120, 1579

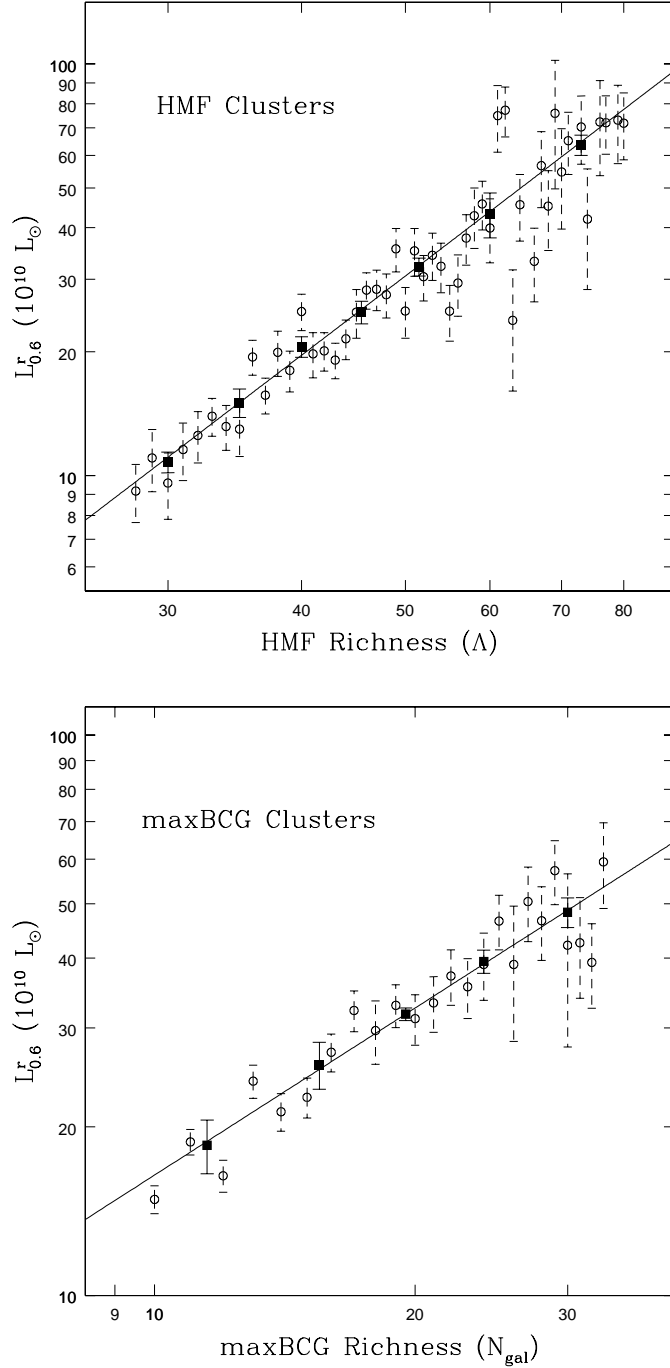


Fig. 1.— Observed cluster luminosity versus richness for HMF and maxBCG clusters. Cluster luminosity is observed in the r -band, within a radius of $0.6 h^{-1}$ Mpc, for stacked clusters at a given richness. The luminosities are k -corrected, background subtracted, and integrated down to $M_r = -19.8$. Dark squares represent binned data. (See section 3)

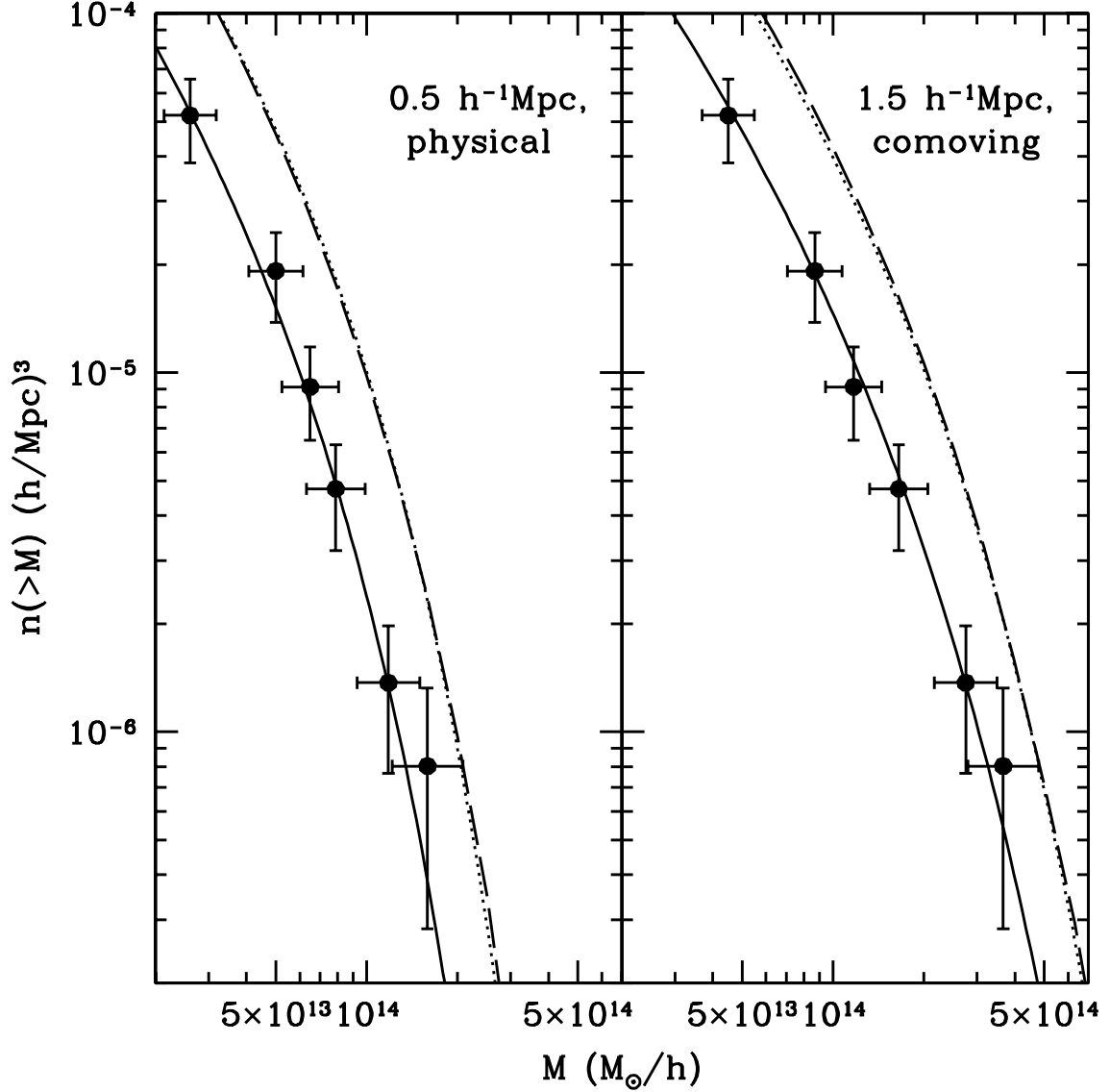


Fig. 2.— The HMF cluster mass function for masses within radii of $0.5 h^{-1}$ Mpc (left panel) and $1.5 h^{-1}$ Mpc comoving (right panel). The solid line is the best-fit analytic mass function (determined at $0.6 h^{-1}$ Mpc and extrapolated to the appropriate radius assuming an NFW profile), with $\Omega_m=0.175$ and $\sigma_8=0.92$. In each panel the dashed line is the mass function measured from an N-body simulation of the concordance LCDM model with $\Omega_m=0.30$ and $\sigma_8=0.90$; the dotted line is the analytic prediction for this simulated cosmology.

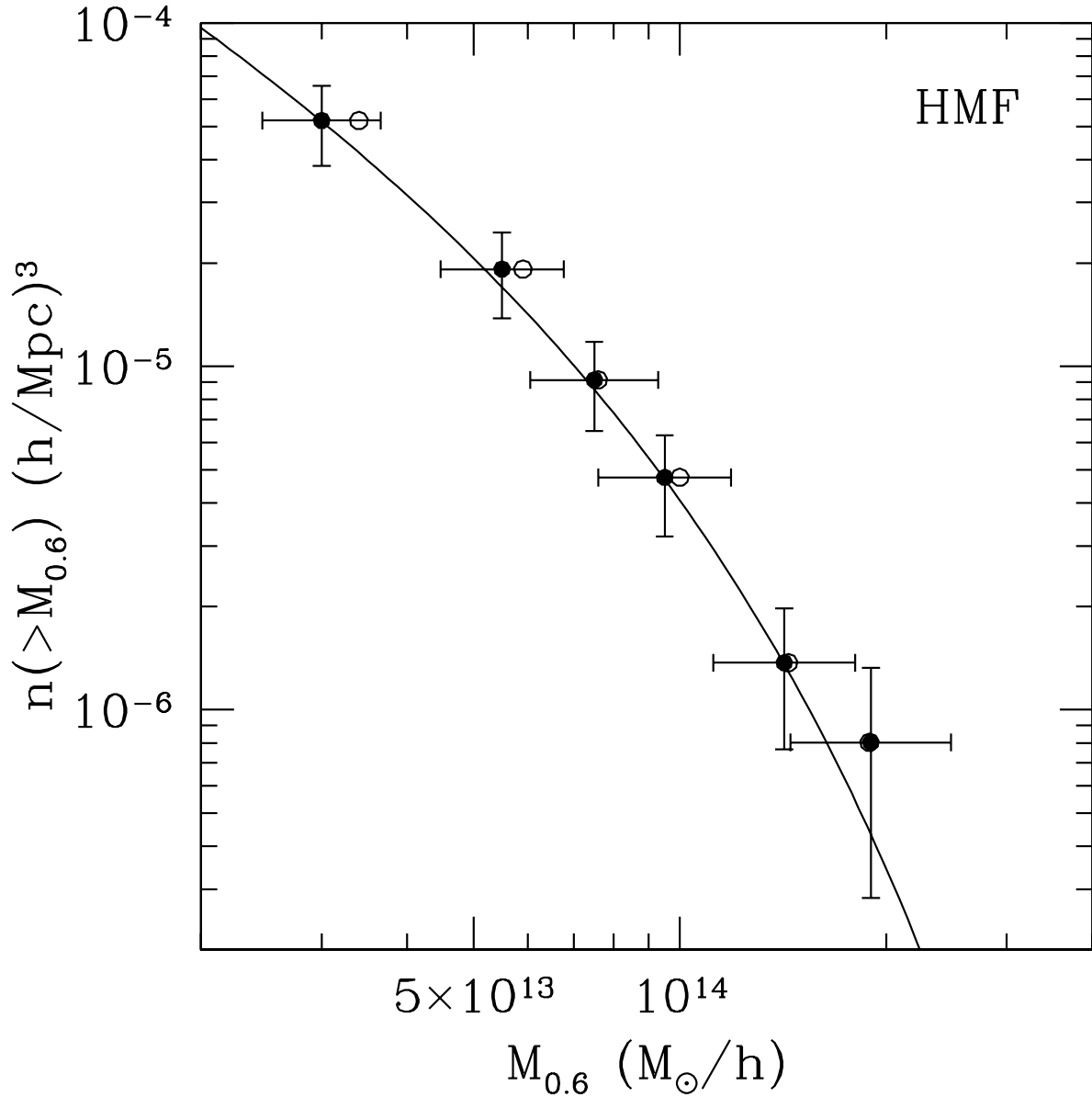


Fig. 3.— The HMF cluster mass function, showing masses (within $0.6 h^{-1}$ Mpc) determined from both the luminosity – mass calibration (filled circles) and the independent velocity dispersion – mass relation (open circles). (The observed cluster abundances assume a volume corresponding to a flat $\Omega_m = 0.2$ cosmology.) The best-fit analytic model, with $\Omega_m = 0.175$ and $\sigma_8 = 0.92$, is shown by the solid line.

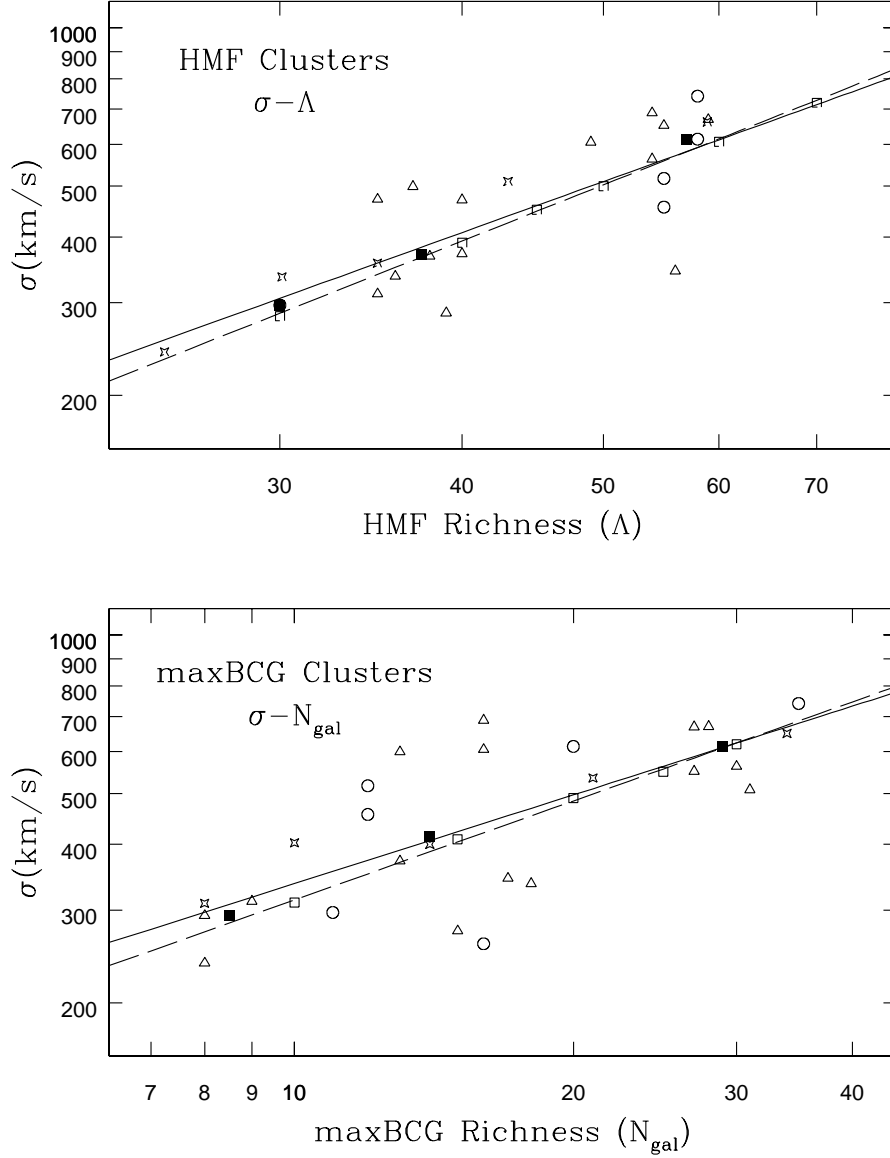


Fig. 4.— Relation between observed cluster velocity dispersion σ and cluster richness (triangles are SDSS observed velocity dispersions, circles are Abell clusters, dark squares are medians, and solid line is best fit to the velocity data. Stars represent SDSS observation of stacked cluster data, shown for comparison only). The median observed velocities are compared with the velocity determined from the cluster masses derived from the mean richness–luminosity–mass relation used in Section 3 (represented by open squares and the best-fit dashed line). A good agreement between the two methods is seen.

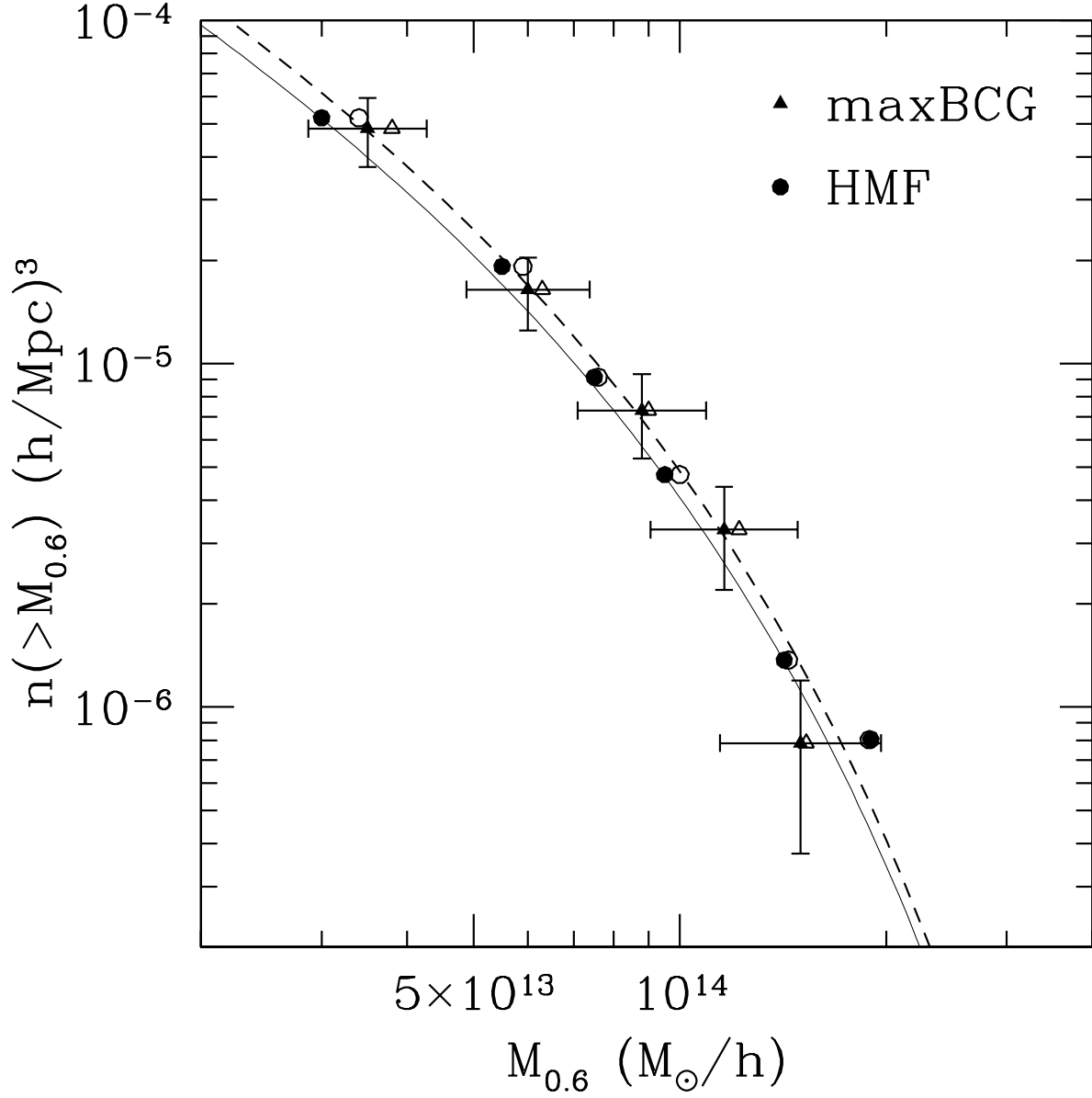


Fig. 5.— The maxBCG and the HMF cluster mass functions, showing masses determined from both luminosity – mass relation (solid triangles: maxBCG; solid circles: HMF) and velocity dispersion – mass relation (open triangles: maxBCG; open circles: HMF). The best-fit analytic models are shown by the dashed line (maxBCG; $\Omega_m = 0.195, \sigma_8 = 0.90$), and solid line (HMF; $\Omega_m = 0.175, \sigma_8 = 0.92$; as in Figure 2).

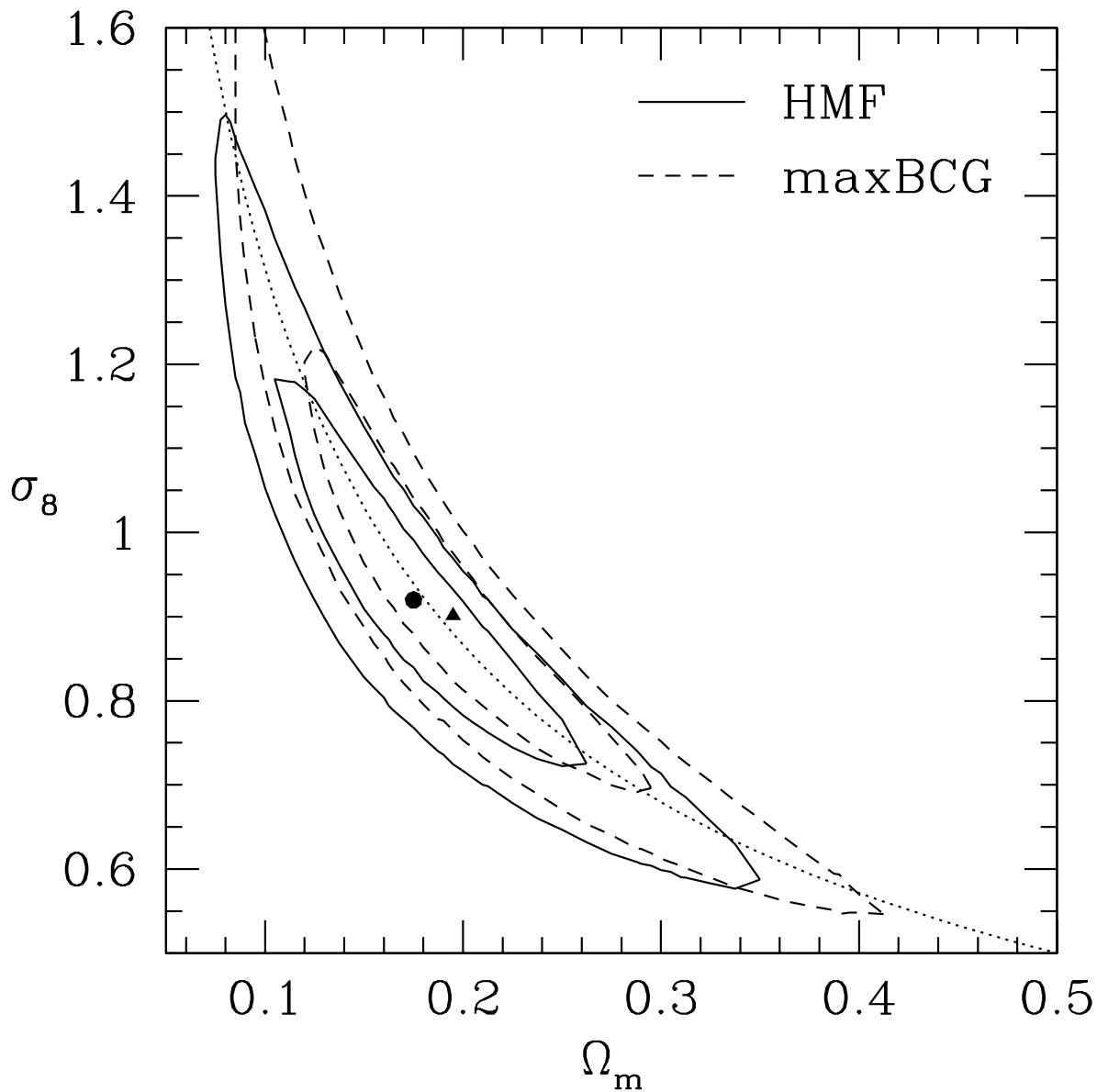


Fig. 6.— Allowed Ω_m - σ_8 range: one- and two- σ confidence contours for HMF (solid lines) and maxBCG clusters (dashed lines). The dotted curve is the best-fit relation $\sigma_8 = 0.33\Omega_m^{-0.6} \simeq (\frac{0.16}{\Omega_m})^{0.6}$. The best-fit Ω_m , σ_8 values are shown by the dark circle (HMF) and triangle (maxBCG).

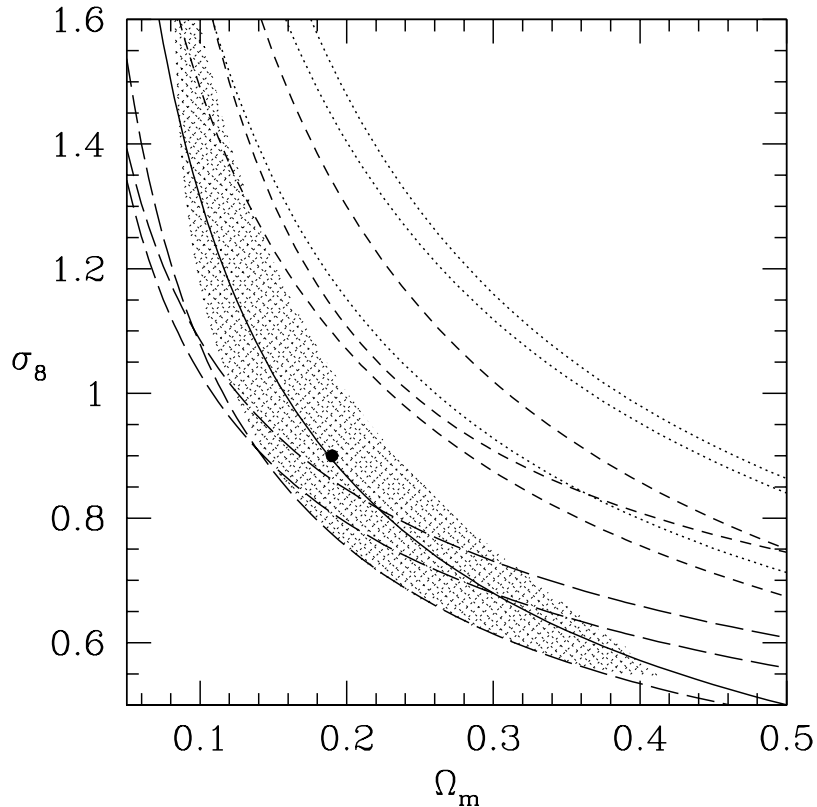


Fig. 7.— Comparison with previous results: the allowed Ω_m - σ_8 range from our present SDSS mass function is compared with previous results from cluster temperature functions. The current $2\text{-}\sigma$ constraints (from Fig. 6) are represented by the shaded area, with the best-fit relation shown by the solid line, and the best-fit parameters ($\Omega_m = 0.19$, $\sigma_8 = 0.9$) indicated by the filled circle. The various dotted and dashed curves represent the best-fit relations given by previous work (for clarity, the allowed width of each range is not shown; it typically corresponds to $\pm \sim 10\%$ in σ_8 at a given Ω_m). Dotted lines represent early results (White, Efstathiou, & Frenk 1993; Viana & Liddle 1996; Eke, Cole, & Frenk 1996; top to bottom); short-dashed lines are mostly re-analyses of same/similar early data (Pierpaoli et al. 2001; Oukbir & Arnaud 2001; Protty Wu 2001; top to bottom); long-dashed lines represent lower normalization relations obtained from recent analyses and/or recent samples (Seljak 2002; Reiprich & Bohringer 2002; Viana, Nichol, & Liddle 2002; top to bottom at higher Ω_m). Weak lensing analyses on large scales (Sections 1, 4; not shown) yield results that are mostly near the high range of these curves, with Hoekstra et al. 2002 fitting well on our best-fit relation.